Noise in voltage-biased scaled semiconductor laser diodes

S. M. K. Thiyagarajan and A. F. J. Levi
Department of Electrical Engineering
University of Southern California
Los Angeles, California 90089-1111

Abstract

Calculations predict a strong negative feedback between the chemical potential and injected current in scaled laser diodes excited by constant voltage through a series resistance. This causes the Relative Intensity Noise (RIN) of lasing emission in scaled laser diodes to be significantly enhanced at low frequencies and suppressed at the relaxation oscillation frequency.

Scaling (reducing the size of) a laser diode resonant cavity and active volume decreases the number of photons and electrons in the device. This reduction increases RIN. In addition, RIN in a scaled laser diode depends critically on whether the device is biased with a current or a voltage.

Early work on RIN reduction investigated electrically pumped conventional laser diodes with "quiet" current sources [1,2]. Calculations of RIN as a function of spontaneous emission factor, β have also been reported [3]. In contrast to these previous studies, we report for the first time, an intrinsic feedback mechanism which dominates RIN behavior in scaled laser diodes under voltage bias. This mechanism is negligible in conventional laser diodes and becomes pronounced only when device dimensions are scaled.

Inset to Fig. 1 schematically illustrates a laser diode under (i) constant current and (ii) constant voltage bias. For a constant voltage source with output V_0 the instantaneous current $I = (V_0\text{-}V_D)/R_s$, where V_D is the voltage drop across the diode and R_s is a series resistance which includes any contact resistance. A random increase in current from its mean value I_0 increases instantaneous voltage across R_s and reduces voltage across the laser diode. This decreases current flowing through the diode and the circuit, thereby damping the current fluctuation. To explore this feedback mechanism in scaled laser diodes we use Langevin equations [4],

$$\frac{dS}{dt} = (G - \kappa)S + \beta R_{sp} + F_s(t) \tag{1}$$

and

$$\frac{dN}{dt} = \left(\frac{I}{e}\right) - GS - \gamma_e N + F_e(t) \tag{2}$$

where S and N are the total photon and carrier numbers in the cavity, G (κ) is the gain (loss), β is the spontaneous emission factor, γ_e is the carrier recombination rate, and e is the charge of an electron. R_{sp} accounts for spontaneous emission into all optical modes and $F_s(t)$, $F_e(t)$ are Langevin noise terms. In the Markovian approximation the auto-correlation and cross-correlation functions are given by

$$\langle F_s(t)F_s(t')\rangle = ((G + \kappa)S + \beta R_{sp})\delta(t - t') \tag{3}$$

$$\langle F_e(t)F_e(t')\rangle = (I/e + GS + \gamma_e N)\delta(t - t') \tag{4}$$

$$\langle F_s(t)F_e(t')\rangle = (-(GS + \beta R_{sp}))\delta(t - t') \quad (5)$$

The negative sign in Eqn. (5) indicates that $F_s(t)$ and $F_e(t)$ are anti-correlated. Thermal noise in the series resistor R_s is accounted for by replacing the I/e diode shot-noise term in Eqn. (4) with $(I/e)+(4k_BT/(e^2R_s))$, where k_B is the Boltzmann constant and T is the temperature of R_s.

Before proceeding, it is worth mentioning a detail. The noise terms in Eqns. (3 - 5) are obtained directly from the rates on the right hand side of Eqn. (1) for the S reservoir and Eqn. (2) for the N reservoir. Although in scaled devices correlation between individual noise terms such as $\gamma_e N$ and GS may be important, correlation of fluctuations within a reservoir is ignored. This may be considered reasonable since anti-correlation between noise sources in a given reservoir does not significantly alter the conclusions of the present work. Infact, it has previously been noted [5] that elimination of the I/e term in Eqn. (4) at best results in only a 3 dB reduction in RIN. For ease of comparison, we keep this term in both the current and voltage bias cases studied here.

For small fluctuations we assume V_D (and the difference in chemical potential across the diode) varies linearly as $V_D = V_{D0} + (\zeta/\upsilon)N$ where V_{D0} is the carrier independent voltage term and the carrier dependent term has slope of ζ/υ, where υ is the active volume of the device. The mean steady-state value for S (N) is S_0 (N_0) while the magnitude of the Fourier component of S (N) at RF angular frequency ω is $\delta S_{V(I)}(\omega)$ ($\delta N_{V(I)}(\omega)$). The subscript V (I) is used to denote constant voltage (constant current) bias. Linearizing the dynamical Eqns. (1) and (2) and neglecting gain saturation, gives

$$\delta N_V(\omega)\left(j\omega + \frac{\zeta}{e\upsilon R_s} + G_N S_0 + \gamma_e + \gamma_e' N_0\right) = F_e(\omega) - G\delta S_V(\omega), \quad (6)$$

$$\delta S_V(\omega) = \frac{F_e(\omega)\left(G_N S_0 + \frac{2\beta B N_0}{\upsilon}\right) + F_s(\omega)\left(j\omega + \frac{\zeta}{e\upsilon R_s} + G_N S_0 + \gamma_e + \gamma_e' N_0\right)}{\left(j\omega\left(\frac{\zeta}{e\upsilon R_s} + G_N S_0 + \gamma_e + \gamma_e' N_0\right) - \omega^2 + GG_N S_0 + G\frac{2\beta B N_0}{\upsilon}\right)}, \quad (7)$$

where $\gamma_e' \equiv \frac{d\gamma_e}{dN}$ and $F_e(\omega)$ and $F_s(\omega)$ are the Fourier components at ω of $F_e(t)$ and $F_s(t)$ respectively. Similarly, for the constant current bias

$$\delta S_I(\omega) = \frac{F_e(\omega)\left(G_N S_0 + \frac{2\beta B N_0}{\upsilon}\right) + F_s(\omega)(j\omega + G_N S_0 + \gamma_e + \gamma_e' N_0)}{\left(j\omega(G_N S_0 + \gamma_e + \gamma_e' N_0) - \omega^2 + G G_N S_0 + G\frac{2\beta B N_0}{\upsilon}\right)}. \quad (8)$$

$RIN \equiv \lim(\tau \to \infty)\frac{1}{\tau}\left|\frac{\delta S(\omega))}{S_0}\right|^2$ is calculated using Eqns. (7) and (8) for the constant voltage and constant current bias case respectively.

A linear model of optical gain, $G = \Gamma g_{slope} v_g(N/\upsilon - N_{tr}/\upsilon)$, is used with gain slope $g_{slope} = 5.0X10^{-16}$ cm^2, transparency carrier density $N_{tr}/\upsilon = 1.0X10^{18}$ cm^{-3}, mode confinement factor $\Gamma = 0.1$, photon group velocity $v_g = 8.1X10^9$ cm s^{-1} and lasing wavelength $\lambda = 1300$ nm. Internal loss is 10 cm^{-1}, $\gamma_e N = R_{sp} = BN^2/\upsilon$ where the radiative recombination coefficient $B = 1X10^{-10}$ cm^{3}s^{-1}, spontaneous emission factor $\beta = 10^{-4}$, and $\zeta = 5X10^{-20}$ cm^{3}V, unless specified otherwise. These values are typical of InGaAsP lasers [6-7]. Although the number of electromagnetic resonances in a cavity changes when scaling photon cavity dimensions, we will show that a change in β does not significantly alter the main conclusions of this work. In addition, the presence or absence of anti-correlation between $F_s(t)$ and $F_e(t)$ on RIN also does not change the main conclusions of this work.

Figure 1(a) shows calculated RIN characteristics for a current biased $\upsilon = 300X2X0.05$ μm^3 conventional cleaved facet edge-emitting laser at T = 0 K. Facet reflectivity R = 0.3, threshold current $I_{th} = 1.84$ mA and the resonant optical cavity is 300 μm long. We consider mean injection in current $I_0 = 4XI_{th}$ as representative of a practical laser diode operating point. With $I_0 = 4XI_{th} = 7.36$ mA, $S_0 = 9.5X10^4$, and $N_0 = 5.9X10^7$. For $\zeta = 5X10^{-20}$ cm^{3}V there is negligible difference between current and voltage bias with $R_s = 100\ \Omega$. This is not shown in Fig. 1(a) as the curves lie on top of one another. Similarly, because diode shot noise dominates resistor thermal (Johnson) noise ($2eI_0 > 4k_BT/R_s$), there is essentially no difference between T = 0 K and T = 300 K.

Figure 1(b) shows calculated RIN characteristics for a $\upsilon = 1X1X1$ μm^3 microlaser. Mirror reflec-

tivity R = 0.999, I_{th} = 32 μA and the resonant optical cavity is 1 μm long. At mean injection current $I_0 = 4XI_{th}$ = 128 μA, $S_0 = 4.0X10^3$, and $N_0 = 1.4X10^6$. Constant current bias and constant voltage bias with R_s = 100 Ω for $\zeta = 5X10^{-20}$ cm^3V at T = 0 K and T = 300 K are considered. Since carriers can not react effectively to a noise perturbation at frequencies well above the relaxation oscillation frequency, ω_R, thermal noise from R_s significantly alters the RIN characteristics only for frequencies near and below ω_R. At a given temperature there is negligible difference between constant current bias and constant voltage bias with $\zeta = 1X10^{-21}$ cm^3V (not shown in the Figure). This is to be expected since in the limit of $\zeta \to 0$, the chemical potential and hence the current in the circuit is independent of the carriers in the medium. Here the injection current is a constant and becomes indistinguishable from the constant current bias case. Further, for a given value of ζ, the difference between voltage and current bias is enhanced for the microlaser compared to the conventional edge-emitting laser. This is attributed to two factors. First, minimum I_0 ($> I_{th}$) is greater in larger devices giving a smaller value of $R_D = V_D/I$. If $R_s >> R_D$ constant voltage bias behaves as a constant current bias since $I = V_0/(R_s+R_D) \sim V_0/R_s \sim$ constant. Second, microlaser active volume for the device of Fig. 1(b) is smaller by a factor of 30 than the conventional laser of Fig. 1(a) leading to a significant difference in their respective N_0 values. Hence, a unit change in microlaser N causes a larger change in carrier density, chemical potential, and a larger feedback effect.

For the current bias cases in Fig. 1(a) and (b) there is a significant increase in RIN for the microlaser compared to the conventional laser. This is because the absolute number of photons in the microlaser is smaller ($S_0 = 4.0X10^3$) and hence relative fluctuations are larger than that of the conventional laser ($S_0 = 9.5X10^4$).

Maximum noise suppression (enhancement) is caused by negative (positive) feedback. This occurs when the phase difference between cause (noise source F_e and or F_s) and effect (the feedback term leading to a change in current injection) is π (2π) radians. The phase difference between carriers and noise source is calculated using Eqns. (6) and (7). As shown in Fig. 2(a), at frequencies near ω_R carriers are in phase with the F_e noise term causing the negative feedback

term to suppress the contribution of F_e noise to RIN. However, in the low-frequency region (Fig. 2(b)) carriers and F_s are π radians out of phase causing the feedback term (which is π radians out of phase with carriers) to enhance the contribution of F_s noise to RIN. At low frequencies, suppression of the contribution of F_e noise to RIN is minimal because the carrier response is ~$3\pi/2$ out of phase with F_e. At or near ω_R carriers lag ~ $3\pi/2$ radians behind F_s noise (not shown in Figure) and the negative feedback does not suppress the contribution of F_s noise to RIN. Hence, the overall effect of constant voltage bias is to suppress RIN near ω_R and to enhance RIN at low frequencies.

Figure 3(a) shows the effect of arbitrarily setting $\langle F_s(t)F_e(t')\rangle = 0$ for the laser of Figure 1(b). Under current bias, the absence of anti-correlation increases RIN in the low-frequency region by approximately 2.7 dB and in the high-frequency region by < 0.1 dB. The effect of anti-correlated noise sources reduce deviation from the mean steady-state value as compared to un-correlated noise sources. Under voltage bias, the absence of the anti-correlation term increases RIN in the low-frequency region by approximately 1.3 dB and in the high-frequency region by < 0.06 dB. Clearly, the presence of anti-correlation between $F_s(t)$ and $F_e(t)$ only enhances the difference in RIN between current bias and voltage bias, thereby retaining the trends discussed above.

Figure 3(b) shows the effect of anti-correlation between $F_s(t)$ and $F_e(t)$ for the device of Fig. 3(a) but with much reduced current bias, $I_0 = 1.1XI_{th} = 36$ μA and $S_0 = 187$. There is essentially no difference between the RIN spectra with and without anti-correlation. This is due to significantly larger RIN values at low frequencies for $I_0 = 1.1XI_{th}$ (Fig. 3(b)) compared to $I_0 = 4XI_{th}$ (Fig. 3(a)).

Shown in Fig. 3(c) is the calculated RIN spectra for the device of Fig. 3(a) with $\beta = 10^{-4}$ and $\beta = 10^{-2}$ under the assumption that β does not change G. The data shows that RIN spectra for current and voltage bias is essentially independent of β.

We obtain photon statistics for the device modeled in Fig. 3(a) by numerical integration of Eqns.

(1) and (2) with the assumption $\langle F_s(t)F_e(t')\rangle = 0$. As shown in Fig. 4(a), the same feedback effect for the voltage-biased microlaser reduces the variance of photon probability by a factor of more than 3 compared to the current-bias case (factor less than 1.01 between current and voltage bias is observed for the conventional laser diode of Fig. 1(a)). Fig. 4(b) shows the time domain response of the microlaser under current bias and voltage bias, clearly showing a suppression in the variation from $S_0 = 4.0X10^3$.

Figure 5 shows the effect on RIN of further reduction in microlaser active volume to υ = 1X0.2X0.2 μm^3. In this case mirror reflectivity of the 1 μm long cavity is R=0.999 and I_{th} = 1.5 μA. The device is biased with $I_0 = 4XI_{th} = 6$ μA such that $S_0 = 198$ and $N_0 = 5.59X10^4$. From Figure 5, it is clear that voltage bias *dramatically* enhances low-frequency noise and suppresses noise near the relaxation oscillation frequency.

In conclusion, *reducing* laser diode dimensions increases the negative feedback between chemical potential and injected current in a voltage biased device. In addition, RIN at low frequencies is enhanced while RIN at or near ω_R is suppressed. The challenge for future work will be developing a theoretical formalism to self-consistently model the microscopic processes which govern scaled laser diode characteristics. Key to any such approach is the self-consistent calculation in which the electronic and optical properties are treated on an equal footing. The semiconductor Maxwell-Bloch equations of Ref. [8] is an example of work in this direction. Such a treatment should be capable of modeling the expected enhancement of the non-linearities in ultra-small high-Q microcavities which will lead to a breakdown of the Markovian approximation.

Acknowledgements: This work is supported in part by the Joint Services Electronics Program under contract #F49620-94-0022, the DARPA Ultra-II / Air Force Office of Scientific Research program under contract #F49620-97-1-0438 and HOTC subcontact #KK8019.

References:

[1] Y. Yamamoto and S. Machida, Phys. Rev. A, 1987, **35**, 5114.

[2] Y.Yamamoto, S. Machida and O. Nilsson "Coherence, Amplification and Quantum Effects in Semiconductor Lasers", Edited by Y. Yamamoto, Wiley-Interscience, New York, 1991, pp.461-537.

[3] G. P. Agrawal and G. R. Gray, Appl. Phys. Lett., 1991, **59**, 399.

[4] D. Marcuse, IEEE J. Quantum Electron., 1984, **QE-20**, 1139 and 1148 .

[5] Y. Yamamoto and S. Machida, Phys. Rev. A, 1986, **34**, 4025.

[6] G. P. Agrawal and N. K. Dutta, "Semiconductor Lasers", 2nd edn., Van Nostrand Reinhold, New York, 1993.

[7] S. L. Chuang, J. O'Gorman, and A. F. J. Levi, IEEE J. Quantum Electron., 1993, **QE-29**, 1631.

[8] S. Bischoff, A. Knorr and S. W. Koch, Phys. Rev. B, 1997, **55**, 7715.

Figure captions

Figure 1: (a) Calculated RIN spectra at T = 0 K for a υ = 300X2X0.05 μm^3 cleaved facet (R = 0.3) edge-emitting laser under current bias with $I_0 = 4XI_{th}$ = 7.36 mA, $S_0 = 9.5X10^4$, and $N_0 = 5.9X10^7$. RIN spectra for the current biased laser at T = 300 K and the voltage biased laser at T = 0 K differ minimally from the current biased laser at T = 0 K and hence is not shown in Figure. Inset shows electrical excitation schemes (i) current bias and (ii) voltage bias. (b) Calculated RIN spectra for a υ = 1X1X1 μm^3 microlaser with R = 0.999, $I_0 = 4XI_{th}$ = 128 μA, $S_0 = 4.0X10^3$, $N_0 = 1.4X10^6$ and R_s = 100 Ω for current bias at T = 0 K (dashed curve) and T = 300 K (solid curve) and voltage bias with $\zeta = 5X10^{-20}$ cm^3V at T = 0 K (dashed curve) and T = 300 K (solid curve).

Figure 2: Illustration in time-domain of the noise term (cause), carriers, and feedback (i.e. change in current injection) when (a) photon noise F_s = 0, at or near ω_R and (b) carrier noise F_e = 0, at frequencies well below ω_R.

Figure 3: Calculated RIN spectra at T = 0 K for a υ = 1X1X1 μm^3 microlaser with a 1 μm long resonant cavity, R = 0.999, $N_0 = 1.4X10^6$, and R_s = 100 Ω. (a) RIN spectra at $I_0 = 4XI_{th}$ = 128 μA, $S_0 = 4.0X10^3$, under current bias and voltage bias, with and without cross-correlation between F_s and F_e. (b) RIN spectra at $I_0 = 1.1XI_{th}$ = 36 μA, S_0 = 187, under current bias, with and without cross-correlation between F_s and F_e. (c) Effect of spontaneous emission factor on the RIN spectra under current and voltage bias, when gain is assumed to be independent of spontaneous emission factor.

Figure 4: (a) Results of calculating probability of finding S photons versus number of photons for the microlaser of Fig. 1(b) at T = 0 K. Voltage bias case (solid curve) is more peaked around S_0 than the current bias case (dashed curve). Variance $\langle S^2 \rangle$ of each probability distribution is indicated. Photon statistics are obtained for S using $4X10^6$ consecutive time intervals with a time increment of 10^{-13} s. (b) Time domain response of the number of photons in the cavity, S for the

microlaser at T = 0 K. The variation in S from S_0 is decreased in the voltage bias as compared to the current bias, thereby leading to a smaller variance seen in (a).

Figure 5: Calculated RIN spectra at T = 0 K for a υ = 1X0.2X0.2 μm^3 microlaser under current bias and voltage bias for the different indicated values of ζ. The device has a 1 μm long resonant cavity, R = 0.999, $I_0 = 4XI_{th}$ = 6 μA, S_0 = 198, $N_0 = 5.59X10^4$ and R_s = 100 Ω.

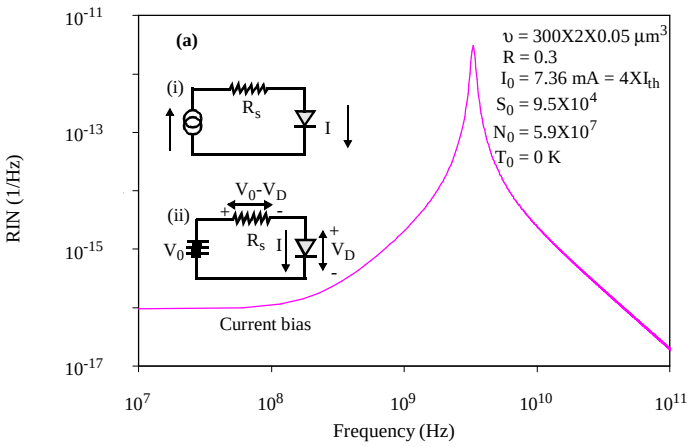
(a)
(i)
R_s
I
V_0-V_D
(ii)
V_0
R_s
I
V_D
Current bias
υ = 300X2X0.05 μm^3
R = 0.3
I_0 = 7.36 mA = 4XI_{th}
S_0 = 9.5X10^4
N_0 = 5.9X10^7
T_0 = 0 K
RIN (1/Hz)
10^{-11}
10^{-13}
10^{-15}
10^{-17}
10^7
10^8
10^9
10^{10}
10^{11}
Frequency (Hz)

Figure 1(a)

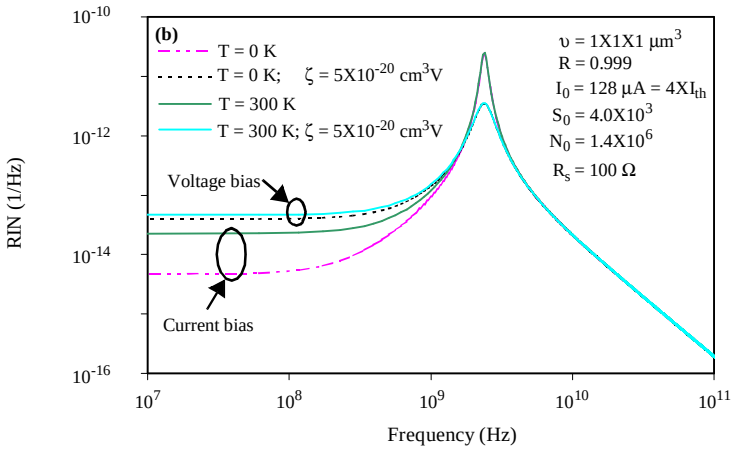
(b)
T = 0 K
T = 0 K; ζ = 5X10^-20 cm^3V
T = 300 K
T = 300 K; ζ = 5X10^-20 cm^3V
υ = 1X1X1 μm^3
R = 0.999
I0 = 128 μA = 4XIth
S0 = 4.0X10^3
N0 = 1.4X10^6
Rs = 100 Ω
Voltage bias
Current bias
RIN (1/Hz)
Frequency (Hz)
10^-10
10^-12
10^-14
10^-16
10^7
10^8
10^9
10^10
10^11

Figure 1(b)

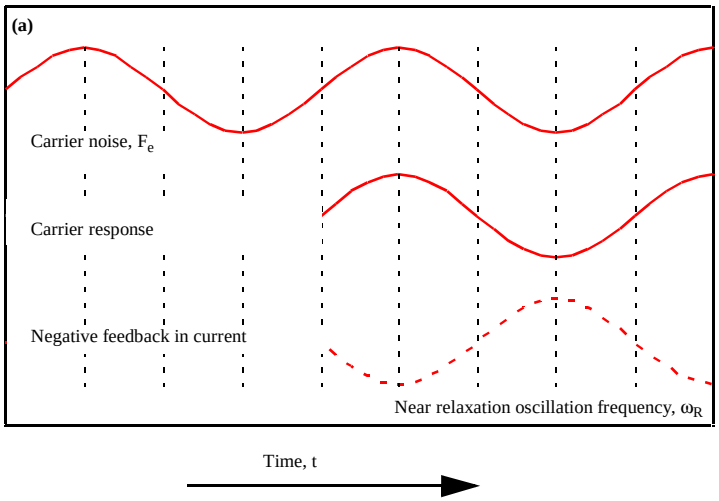
(a)
Carrier noise, F_e
Carrier response
Negative feedback in current
Near relaxation oscillation frequency, ω_R
Time, t

Figure 2(a)

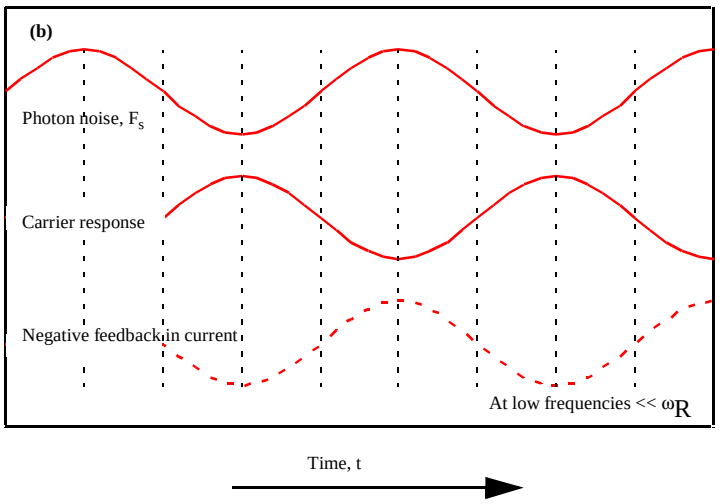
(b)
Photon noise, F_s
Carrier response
Negative feedback in current
At low frequencies << ω_R
Time, t

Figure 2(b)

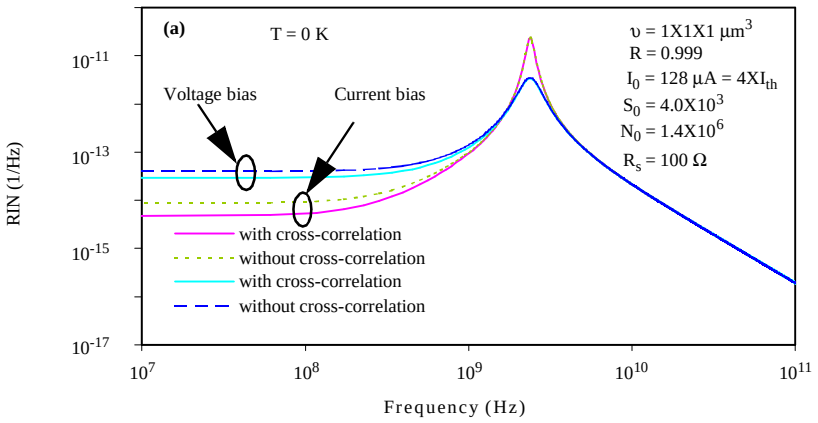
(a)
T = 0 K
υ = 1X1X1 μm3
R = 0.999
I0 = 128 μA = 4XIth
S0 = 4.0X10^3
N0 = 1.4X10^6
Rs = 100 Ω
Voltage bias
Current bias
with cross-correlation
without cross-correlation
with cross-correlation
without cross-correlation
RIN (1/Hz)
10^-11
10^-13
10^-15
10^-17
10^7
10^8
10^9
10^10
10^11
Frequency (Hz)

Figure 3(a)

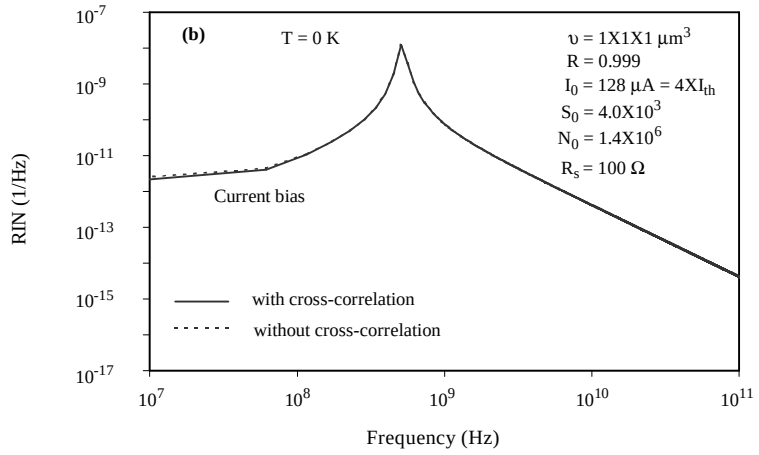
(b)
T = 0 K
υ = 1X1X1 μm3
R = 0.999
I0 = 128 μA = 4XIth
S0 = 4.0X103
N0 = 1.4X106
Rs = 100 Ω
Current bias
with cross-correlation
without cross-correlation
RIN (1/Hz)
Frequency (Hz)
10-7
10-9
10-11
10-13
10-15
10-17
107
108
109
1010
1011

Figure 3(b)

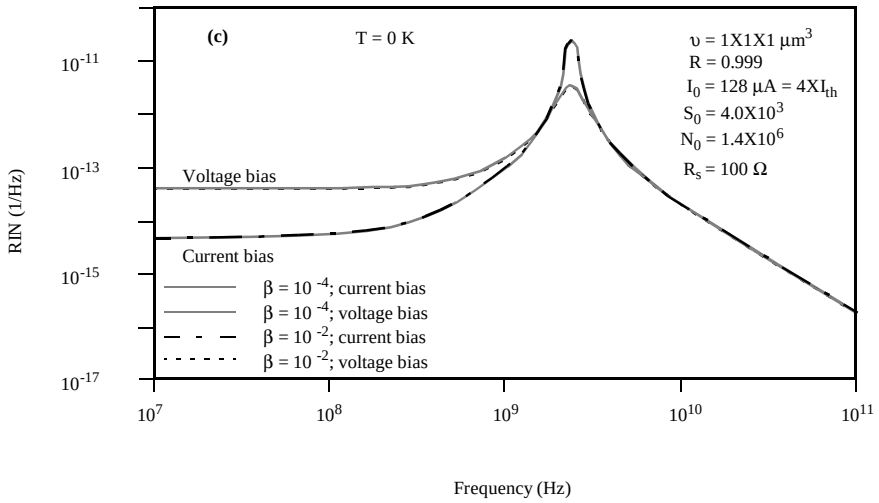
(c)
T = 0 K
υ = 1X1X1 μm3
R = 0.999
I0 = 128 μA = 4XIth
S0 = 4.0X103
N0 = 1.4X106
Rs = 100 Ω
Voltage bias
Current bias
β = 10 -4; current bias
β = 10 -4; voltage bias
β = 10 -2; current bias
β = 10 -2; voltage bias
RIN (1/Hz)
10-11
10-13
10-15
10-17
107
108
109
1010
1011
Frequency (Hz)

Figure 3(c)

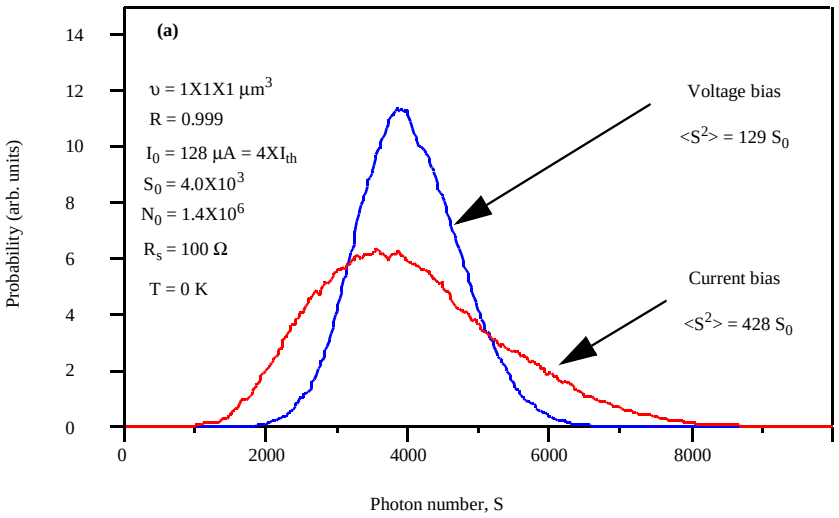
(a)
υ = 1X1X1 μm3
R = 0.999
I0 = 128 μA = 4XIth
S0 = 4.0X103
N0 = 1.4X106
Rs = 100 Ω
T = 0 K
Voltage bias
<S2> = 129 S0
Current bias
<S2> = 428 S0
Probability (arb. units)
Photon number, S
0
2
4
6
8
10
12
14
0
2000
4000
6000
8000

Figure 4(a)

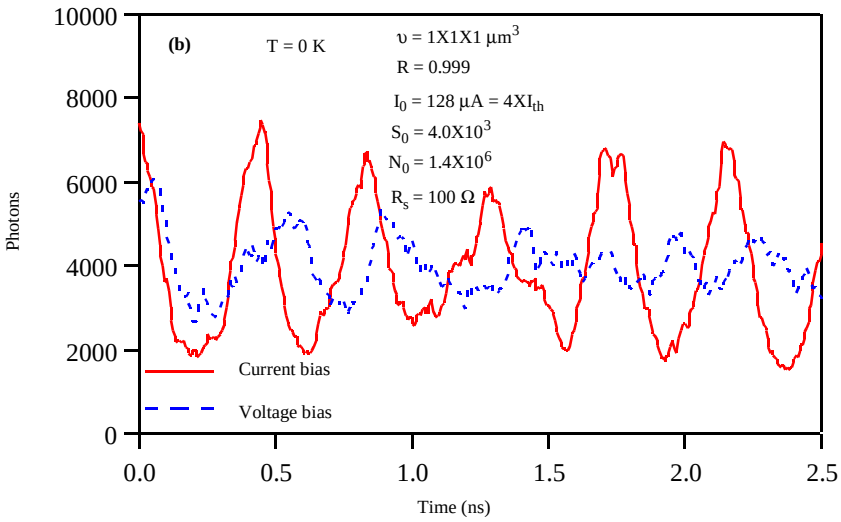
(b)
T = 0 K
υ = 1X1X1 μm3
R = 0.999
I0 = 128 μA = 4XIth
S0 = 4.0X103
N0 = 1.4X106
Rs = 100 Ω
Current bias
Voltage bias
Photons
Time (ns)
10000
8000
6000
4000
2000
0
0.0
0.5
1.0
1.5
2.0
2.5

Figure 4(b)

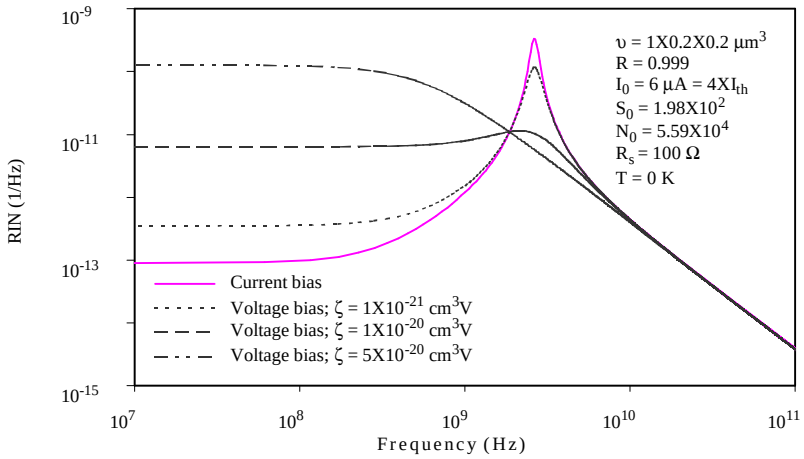
10^{-9}
10^{-11}
10^{-13}
10^{-15}
RIN (1/Hz)
10^{7}
10^{8}
10^{9}
10^{10}
10^{11}
Frequency (Hz)
υ = 1X0.2X0.2 μm^3
R = 0.999
I_0 = 6 μA = 4XI_{th}
S_0 = 1.98X10^2
N_0 = 5.59X10^4
R_s = 100 Ω
T = 0 K
Current bias
Voltage bias; ζ = 1X10^{-21} cm^{3}V
Voltage bias; ζ = 1X10^{-20} cm^{3}V
Voltage bias; ζ = 5X10^{-20} cm^{3}V

Figure 5